Large eddy simulation of propeller crashback

Martin Vyšohlíd & Krishnan Mahesh
Aerospace Engineering & Mechanics
University of Minnesota

mahesh@aem.umn.edu

ABSTRACT

The large eddy simulation methodology is applied to predict the flow around a marine propeller in the forward and crashback modes of operation. A non-dissipative, robust numerical algorithm developed by Mahesh et al.(2004, J. Comput. Phys., 197: 215-240) for unstructured grids was extended to include the effect of rotating frame of reference. The thrust and torque coefficients obtained from the simulation are compared to experimental data and good agreement is observed. The crashback simulations show the presence of a highly unsteady ring-vortex, and unsteady loads on the propeller.

1 INTRODUCTION

Crashback is an extreme operating condition for marine propulsors that often determines propulsor strength, and strongly affects overall maneuverability. Figure 1 shows a schematic of a four-quadrant plot which illustrates the four different modes of propeller operation. Crashback is seen to be the operating condition where the propeller rotates in the reverse direction while the vessel moves in the forward direction. The flow around the propeller during crashback is characterized by massive separation, and large-scale unsteadiness. A prominent feature of the flow is an unsteady ring-vortex in the vicinity of the propeller disk. Jiang et al. [1] performed experiments of propeller crashback which provide PIV data on the ring-vortex, and suggest that the unsteadiness of the ring-vortex is related to the forces experienced by the propeller. Detailed experiments which measure flow velocity in crashback using PIV and LDV were recently performed by Jessup et al. [2].

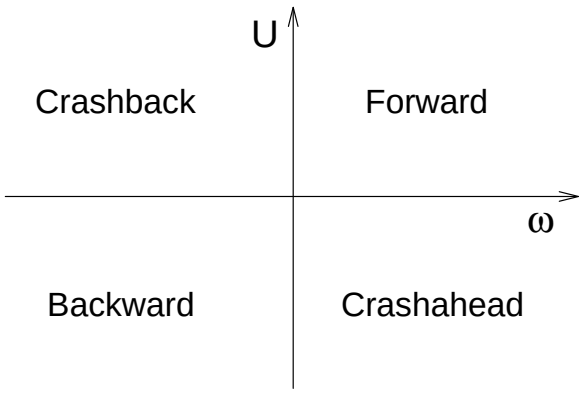

Figure 1: Classification of propeller operation based on the direction of angular velocity ω of the propeller and the direction of the speed of far field flow *U*.

The unsteady Reynolds-averaged Navier-Stokes equations (RANS) represent the state-of-the-art in computational prediction of the viscous flow around propellers [3]–[5]. Currently, RANS appears capable of predicting forward mode and backing; however, significant disagreement with data is observed in crashback and crashahead conditions. For example, Chen & Stern [3] show that RANS is within 5% of experimental data for thrust and torque in the forward mode and within 6.5% when backing, but crashback or crashahead increases the error to 110%. Also the computed results showed only 3% oscillation about the mean while the experiment showed 20%.

An interesting approach to estimate blade loads in crashback using a panel code was suggested by Jiang [7]. This method requires experimental data for the average velocity field in a plane downstream near the propeller. This velocity represents input to the panel code, which only computes the velocity field near the propeller where the flow is reversed and assumed to be similar as in backing mode. The method was applied to propeller P4381 by Jessup [2] and resulted in thrust and torque coefficients within 12% of their experimental measurements. Note that the panel code, which is based on potential flow, cannot predict crashback without experimental input.

It is likely that RANS is unable to adequately predict crashback because of the pervasive large-scale unsteadiness. This paper therefore uses the large-eddy simulation methodology to simulate propeller crashback. LES is a three-dimensional and unsteady computational approach where the Navier-Stokes equations are spatially filtered, and the resolved scales of motion are directly computed while the effect of the unresolved scales is modeled. A known limitation of LES (without wall models) is the near-wall resolution requirements for external flows at high Reynolds numbers. It is hoped that the near-wall resolution is not as critical for the crashback problem which has massive geometry-induced separation. This assumption will be tested by comparison to experimental data.

The paper is organized as follows. Section 2.1 briefly describes the governing equations and numerical method. The propeller geometry and computational grid are outlined in section 2.2. Some results from the computations are shown in section 3. Two cases are considered: one in the forward mode (3.1) and one in the crashback mode of operation (section3.2), respectively. A brief summary in section 4 concludes the paper.

2 SIMULATION DETAILS

2.1 Numerical method

The simulations are performed in a frame of reference that rotates with the propeller. The incompressible Navier-Stokes equations are solved in a rotating coordinate system. The governing equations in a rotating frame can either be written for the velocities measured in a stationary frame or for velocities measured in the rotating frame. The form of the governing equations may be strongly conservative [8] or in a form where system rotation produces a source term e.g. [9]. This paper uses the following form of the governing equations. Note that we solve for the velocities measured in a stationary frame of reference.

$$\frac{\partial u_i}{\partial t} + \frac{\partial}{\partial x_j}(u_i u_j - u_i \varepsilon_{jkl} \omega_k x_l) = -\frac{\partial p}{\partial x_i} - \varepsilon_{ijk} \omega_j u_k + \nu \frac{\partial^2 u_i}{\partial x_j \partial x_j},$$

$$\frac{\partial u_i}{\partial x_i} = 0$$

where x_i are coordinates in the rotating frame, t is time, ω_i is the angular velocity of the rotating frame of reference, u_i is the inertial velocity, p is the pressure, and ν is the kinematic viscosity. Note that the density is absorbed in pressure. Also, the Einstein summation convention is used and ε_{ijk} denotes the permutation symbol.

The LES equations are obtained by spatially filtering (denoted by overbar) the Navier-Stokes equations. The filter is assumed to commute with the spatial and temporal derivatives. Applying the filter and using the approximation

$$\overline{u_i \varepsilon_{jkl} \omega_k x_l} \approx \overline{u}_i \varepsilon_{jkl} \omega_k x_l ,$$

we get

$$\frac{\partial \overline{u}_i}{\partial t} + \frac{\partial}{\partial x_j}(\overline{u}_i \overline{u}_j - \overline{u}_i \varepsilon_{jkl} \omega_k x_l) = -\frac{\partial \overline{p}}{\partial x_i} - \varepsilon_{ijk} \omega_j \overline{u}_k + \nu \frac{\partial^2 \overline{u}_i}{\partial x_j \partial x_j} - \frac{\partial \tau_{ij}}{\partial x_j} ,$$

$$\frac{\partial \overline{u}_i}{\partial x_i} = 0$$

where

$$\tau_{ij} = \overline{u_i u_j} - \overline{u}_i \overline{u}_j$$

is the subgrid stress and is modeled. The dynamic Smagorinski model as proposed by Germano et al. [10] and modified by Lilly [11] is used to model the subgrid stress.

The above equations are solved using a numerical method developed by Mahesh et al. [12] for incompressible flows on unstructured grids. The algorithm is derived to be robust without numerical dissipation. It is a finite-volume approach which stores the Cartesian velocities and the pressure at the centroids of the cells (control volumes) and the face normal velocities are stored independently at the centroids of the faces. A predictor-corrector approach is used. The predicted velocities at the control volume centroids are first obtained and then interpolated to obtain the face-normal velocities. The predicted face normal velocity is projected so that continuity is discretely satisfied. This yields a Poisson equation for pressure which is solved iteratively using a multigrid approach. The pressure field is used to update the Cartesian control volume velocities using a least-squares formulation. Time advancement is implicit and is performed using the Crank-Nicholson scheme. The algorithm has been validated for a variety of problems (see Mahesh et al. [12]) over a range of Reynolds numbers.

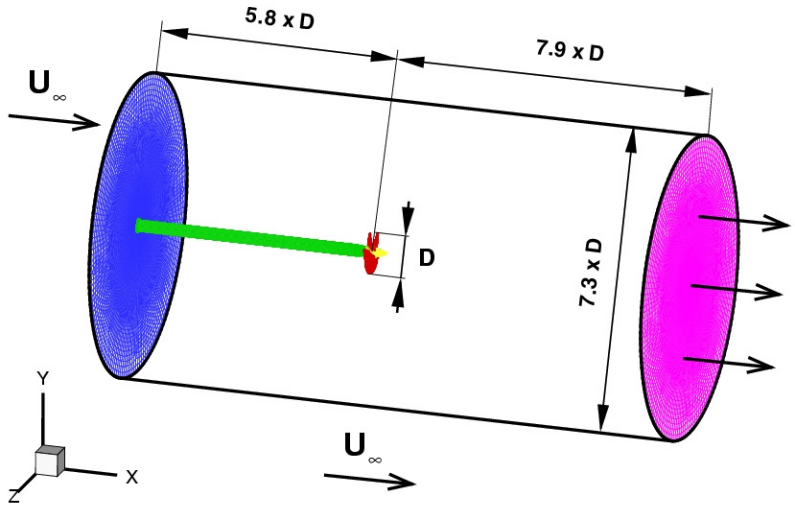

a)

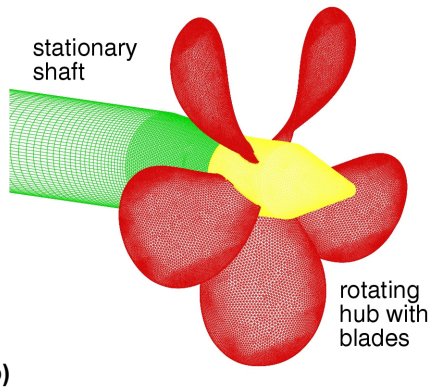

b)

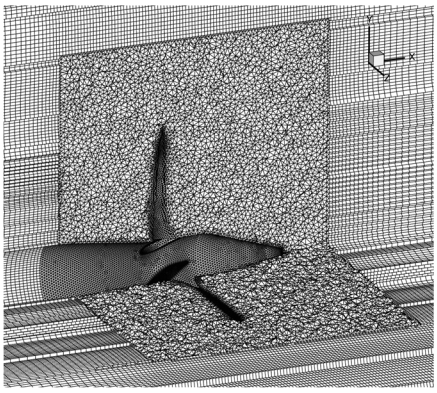

c)

Figure 2: (a) Computational domain, (b) detail view of the propeller (c) mesh in propeller neighborhood.

2.2 Propeller geometry and computational grid

The computations were performed for Propeller 4381, which is a five bladed, right-handed propeller with variable pitch, no skew and rake. The propeller diameter is 12 inches and its geometry was provided by David Taylor Model Basin (Jessup, private communication). A detailed description of the geometry may be found in [2].

Figure 2a shows a schematic of the cylindrical computational domain, whose diameter is 7.3 times the propeller diameter, and length is 13.75 times the propeller diameter. A constant free-stream velocity boundary condition is specified at the inlet and lateral boundaries. Convective velocity boundary conditions are prescribed at the outflow. A detail view of the propeller is shown in Figure 2b. The boundary condition on the propeller, hub and the conical tip are specified using $\mathbf{u} = \omega \times \mathbf{r}$, while the shaft is stationary; i.e. $\mathbf{u} = 0$.

All five blades of the propeller are represented in the computation. The following constraints were imposed on the mesh generation.

- The domain must be large enough in order to avoid effects of constriction. This is most restrictive in the crashback mode.
- There is difference of several orders of magnitude between the size of the trailing edge of a blade and its radius.
- The curvature of trailing edge changes significantly with distance from propeller axis.

A commercial grid generator (Gambit & TGrid, Fluent Corporation) was used for the grid generation. Figure 2c shows the mesh around propeller. Tetrahedral elements are used in the immediate vicinity of the propeller to match the complicated geometry of the blades, while hexahedral elements and prisms are used farther from the propeller. Four layers of prisms were grown on the surfaces of blades in order to improve the resolution of boundary layers on blades. First, the hexahedra and prisms away from the propeller, and surface meshes on the propeller, hub and shaft were created in Gambit. The mesh was then imported into TGrid, and tetrahedral elements were generated around the propeller. The smallest grid size is 1.7×10^{-3} of the propeller diameter, and is found on the edges of the blades; size functions were used to control the growth rate of the grid size to obtain a final mesh with size of approximately 13 million control volumes.

3 RESULTS

3.1 Forward Operation

Simulations were performed in the forward mode at advance ratio J=0.889 for which thrust and torque were measured in a 36 inch water tunnel by Jessup et al. [2], and in a tow-tank by Hecker & Remmers [13] and Jessup (private communication). The advance ratio J is defined as $J = U/(nD)$ where U is the free-stream velocity, n is the propeller rotational speed in rev/s and D is the propeller diameter. The computation was started with uniform flow as the initial condition and with a Reynolds number of 12,000. The Reynolds number is based on the free stream velocity and on the diameter of the propeller. After 6.9 propeller revolutions, the Reynolds number was increased 10 times and after another 2.5 propeller revolutions it was further increased to 894,000 to match the water tunnel experiment. It is shown below that the qualitative features of the flow are captured and that the computed values of thrust and torque show good agreement with experimental measurements in a tow-tank. Also, Reynolds number sensitivity is investigated.

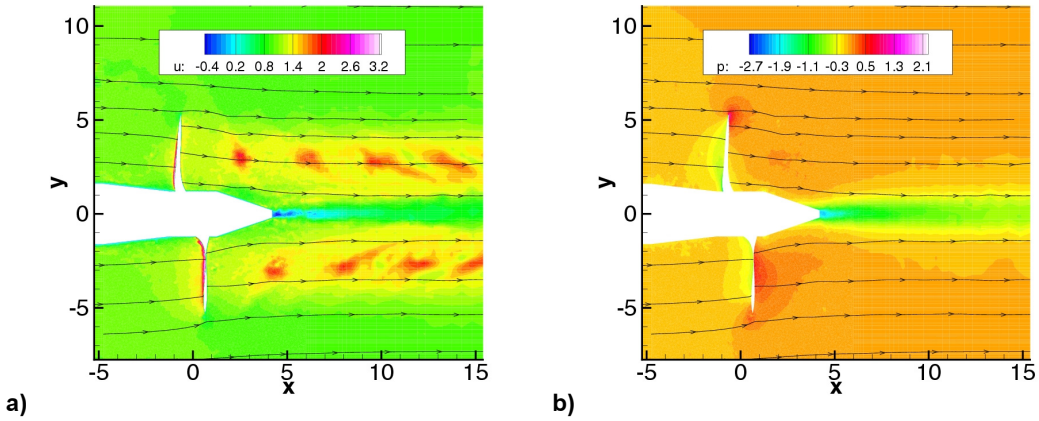

Figure 3: Computed results for forward operation J = 0.889, Re = 894,000: (a) streamlines and contours of velocity normalized by U, (b) streamlines and contours of pressure normalized by ρU^2 .

Figure 3a shows streamlines and axial velocity contours for the design advance ratio J=0.889 at a Reynolds number of 894,000. Note, that the flow is accelerated as it passes through the propeller. As the flow accelerates, the region defined by the streamlines passing through the propeller region (slipstream) contracts. Patches of higher velocity flow correspond to passage of individual blades. The acceleration of fluid is related to the pressure gradient, which in turn determines the thrust and torque on the propeller. Part of the acceleration occurs upstream of the propeller as the pressure on upstream (suction) side of the blade is lower than the ambient pressure, and part of the acceleration occurs downstream as the pressure on downstream (pressure) side of the blade is higher than the ambient pressure. This is documented by the instantaneous pressure contours in figure 3b.

The pressure and viscous stresses over the blades yield thrust T and torque Q, which are non-dimensionalized as

$$K_T = \frac{T}{\rho n^2 D^4}, \qquad K_Q = \frac{Q}{\rho n^2 D^5}$$

where ρ is the fluid density, n is the propeller rotational speed in rev/s and D is the diameter of the propeller. Their values are seen to strongly depend on Reynolds number. The non-dimensional thrust K_T and torque K_Q are plotted in Figure 4a and 4b as they change during the computation. The horizontal axes show time elapsed since the beginning of the computation in propeller revolutions. Note that after each change in Reynolds number, both thrust and torque quickly stabilize and then remain nearly constant with time. The low level of fluctuation in thrust and torque in forward mode is in agreement with experiment. Also shown are the steady experimental values of thrust and torque coefficients measured in a 36 inch water tunnel by Jessup et al. [2], and in a tow-tank by Hecker & Remmers [13] and by Jessup (private communication). The water tunnel results are seen to be lower than the tow-tank values. Note that as the Reynolds number approaches the experimental value, both thrust and torque approach the tow tank results. The computed out-of-plane force (ie. the force orthogonal to the axis of propeller) in Figure 4c is small and it is probably result of a small asymmetry in the computational grid. Experimental and computed values of thrust and torque in forward operation are summarized in Table 1.

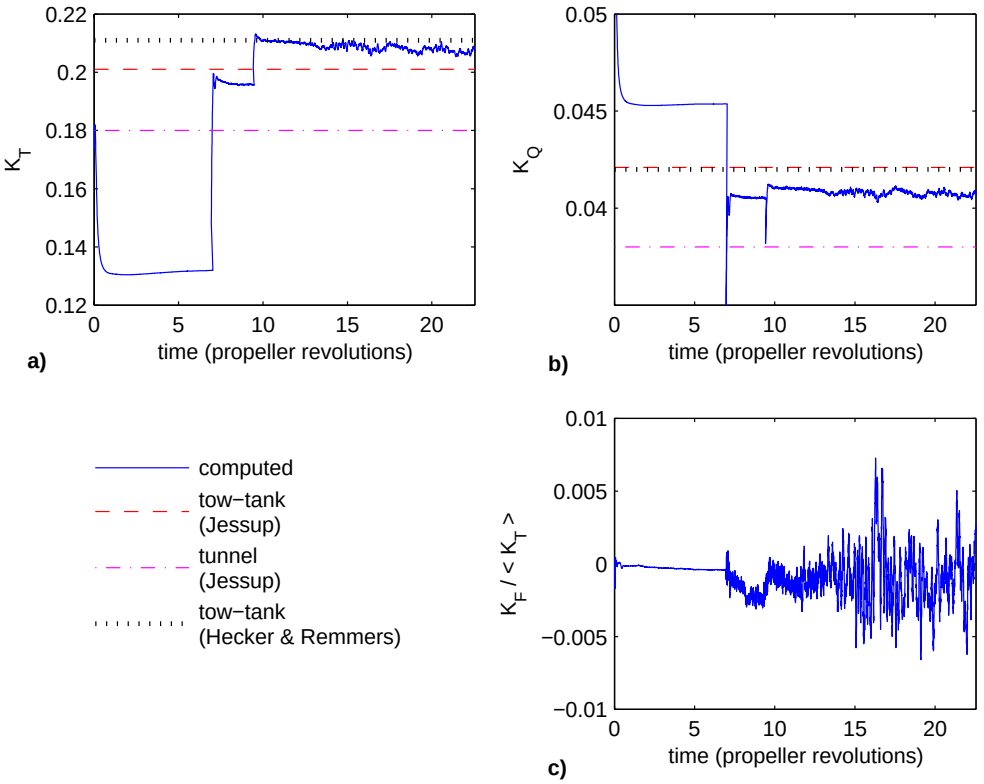

Figure 4: Non-dimensional (a) thrust K_T, (b) torque K_Q and (c) out-of-plane force K_F in *y*-direction normalized by average thrust $<K_T>$ for $J = 0.889$ as they develop during the computation. The computation was started with Reynolds number of 12,000 and then increased in two steps to $Re = 120{,}000$ and experimental $Re = 894{,}000$.

J = 0.889	K_T	K_Q	Re=UD/ν
Tow-tank, Hecker & Remmers [13]	0.211	0.042	6×10^5
Water tunnel, Jessup [2]	0.18	0.038	9×10^5
Tow-tank, Jessup (private communication)	0.201	0.0421	1×10^6
Computed result	0.21	0.041	9×10^5

Table 1: Thrust and torque in forward operation ($J = 0.889$): experimental and computed results. All experimental data, including Hecker & Remmers, were kindly provided by Jessup (private communication) at different advance ratios. The data were interpolated when necessary to obtain the values tabulated above.

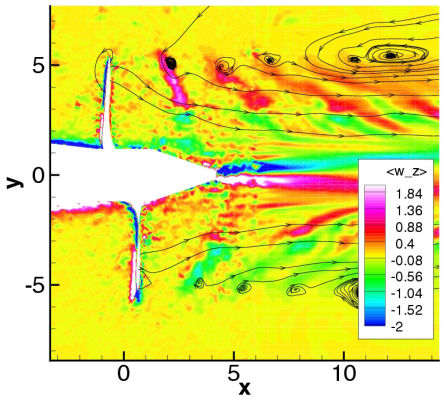

Figure 5: Vorticity contours and streamlines in frame of reference moving with upstream flow. Note the tip vortices and blade wakes. Computed results for forward operation J = 0.889, Re = 894,000 are averaged over 2.8 revolution in the propeller frame of reference.

A propeller blade is a finite twisted wing and therefore there is a trailing tip vortex starting at each blade. As the propeller rotates, the vortices are not straight, but each vortex forms a helix. Intersections of the helical vortices with the axial plane are visible in figure 5, which shows streamlines in a frame of reference moving with the upstream flow, and contours of z-component of vorticity. Figure 5 shows computed results for J=0.889 and Re=894,000 averaged over 2.8 revolutions. A similar plot is shown by the experimental study of Di Felice et al. for a different propeller [14] in Figure 10 of their paper. The computed results show good qualitative agreement with Di Felice et al.'s results. The contours of vorticity reflect locations of the blade wakes. Notice, that as the wake gets further from the propeller, it is stretched. This is due to higher axial velocity closer to the axis. Also seen clearly is the hub vortex.

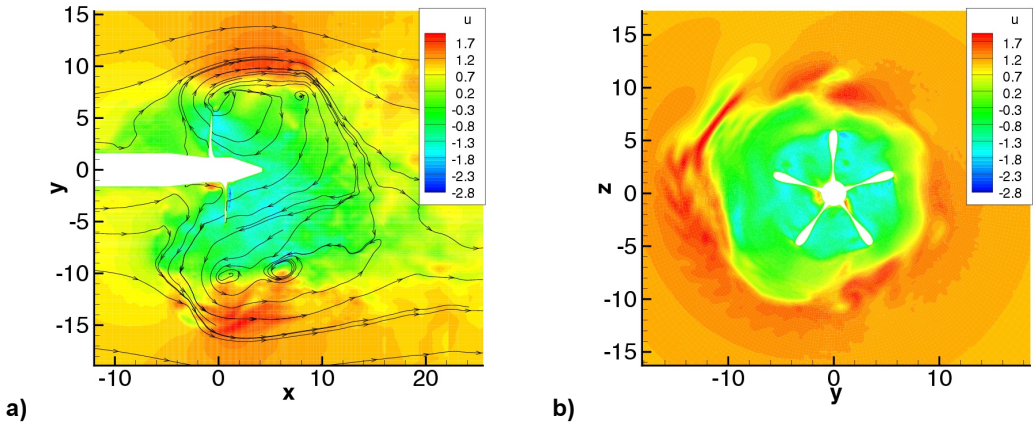

Figure 6: Contours of axial velocity normalized by U and streamlines for crashback J = -0.7, Re = 12,000: (a) side view (b) axial view at $x / D = 0$.

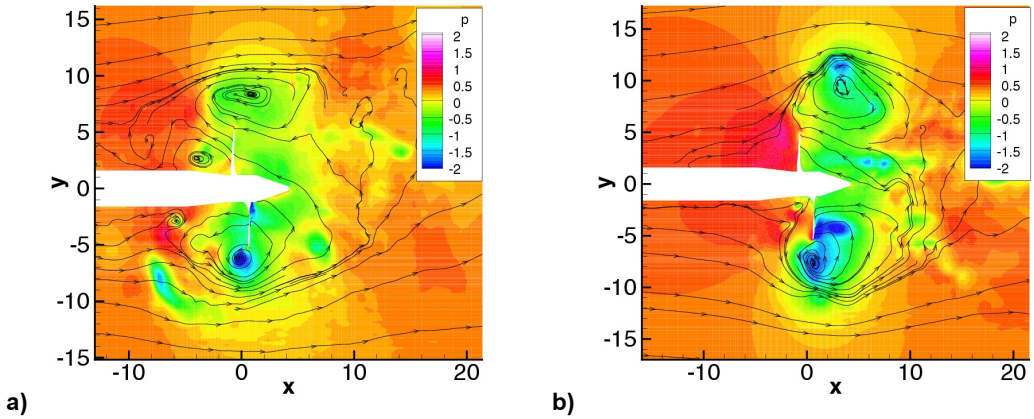

Figure 7: Contours of pressure normalized by ρU^2 and streamlines for crashback J = -0.7 at two different times. Note unsteadiness of the flow.

3.2 Crashback

Simulations were performed under crashback conditions at advance ratio J=-0.7 for which experimental data are available measured in a 36 inch water tunnel by Jessup et al. [2] and in a tow tank by Hecker & Remmers [13] and by Jessup (private communication). The computational grid was the same as that used in forward mode. The simulation was started with a uniform flow as the initial condition with velocity equal to the far field flow velocity. The Reynolds number was Re=1,200, and 336 time steps per revolution were used. After 12 propeller revolutions, the Reynolds number was increased to Re=12,000 and another 24 propeller revolutions were computed using 1680 time steps per revolution.

Crashback is fairly complex, as can be seen by comparing the forward mode in Figure 3 to crashback in Figure 6. Figure 6a shows streamlines and axial velocity contours in a plane along the propeller axis while Figure 6b shows axial velocity contours in a plane perpendicular to the axis of propeller. There is a region of reversed flow close to the propeller in crashback (the blue and green region). This reversed flow interacts with ambient flow and creates a recirculation zone, which is often called a ring vortex. Figure 6b shows the resulting asymmetry of the solution in the various blade passages.

The flow in crashback is highly unsteady as is documented in Figure 7, which shows pressure contours (normalized by ρU^2) and streamlines at two different times. As can be seen from the streamlines, a ring vortex is formed, which moves downstream and upstream, as observed in experiments by Jiang [1]. The ring vortex is closer to the propeller in Figure 7a, which corresponds to lower absolute value of thrust, and the vortex ring is further downstream in Figure 7b, which corresponds to higher absolute value of thrust. This difference in thrust is obvious from the pressure contours – Figure 7b shows higher pressure drop across the blades than Figure 7a. Also note that the sign of the pressure difference on the blades in crashback is opposite than that in forward operation.

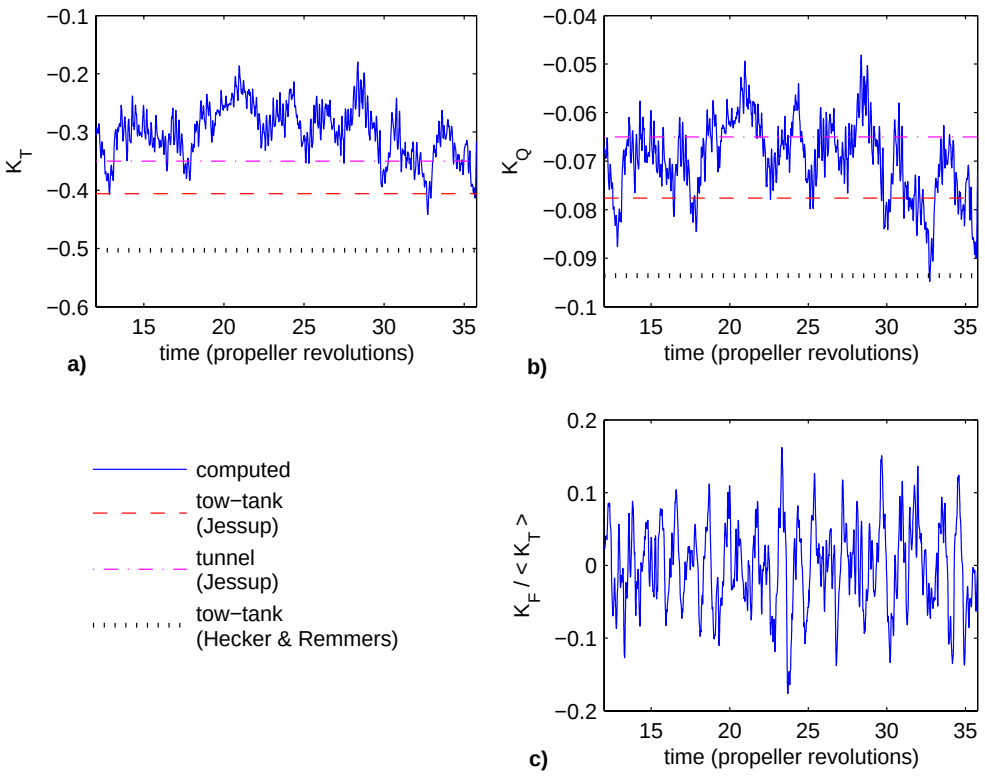

Figure 8: Computed fluctuations of non-dimensional (a) thrust K_T, (b) torque K_Q and (c) out-of-plane force K_F in *y*-direction normalized by average thrust $<K_T>$ for crashback J = -0.7.

J = -0.7	K_T	K_Q	Re=UD/ν
Tow-tank, Hecker & Remmers [13]	-0.503	-0.0936	6×10^5
Water tunnel, Jessup [2]	-0.35	-0.065	9×10^5
Tow-tank, Jessup (private communication)	-0.406	-0.0776	1×10^6
Computed result	see graph		1×10^4

Table 2: Thrust and torque in crashback (J = -0.7): experimental data. All experimental data, including Hecker & Remmers, were kindly provided by Jessup (private communication) at different advance ratios. The data were interpolated when necessary to obtain the values tabulated above.

The asymmetry and unsteadiness of flow is reflected in the blade loads and hence also in thrust, torque and in out-of-plane forces. Figures 8a and 8b show the time history of non-dimensional thrust and torque, respectively. Also shown are the experimental values of average thrust and torque coefficients obtained by Jessup et al. [2] in a water tunnel, and Hecker & Remmers [13] and Jessup (private communication) in a tow tank. The water tunnel results show smaller absolute values of average thrust and torque than tow-tank results. The size of region affected by the propeller is much larger in crashback than in forward mode. We believe that our domain should give results close to open-water performance of the propeller as measured in tow-tank experiments. However, there seems to be significant difference between tow-tank results of Hecker & Remmers and Jessup. The computed results are closer to the results of Jessup, but it would be necessary to compute a longer time sequence to get exact average values of thrust and torque. Future simulations will also increase the Reynolds number to experimental value. Note that the average thrust and torque are in the correct range, and it is promising that the experimentally observed unsteadiness is predicted. Also the time history of computed out-of-plane force normalized by thrust is plotted in Figure 8c. The magnitude and unsteadiness of out of plane forces in crashback is seen to be much larger than in forward operation due to high asymmetry and unsteadiness of the flow in crashback and it is in good agreement with observation of Jiang et al. [1]. The experimental values of thrust and torque are summarized in Table 2.

4 SUMMARY

LES was applied to the turbulent flow around a marine propeller in forward and crashback operation. The qualitative features and the values of thrust and torque for forward operation are in very good agreement with tow-tank experiments of Hecker and Remmers [13]. The crashback simulations show the presence of an unsteady ring vortex, and low frequency unsteadiness in the thrust and torque coefficients. The simulations also predict significantly higher levels of forces orthogonal to the axis of propeller, which would affect overall maneuverability. The results in crashback show reasonable agreement of thrust and torque with tow-tank experiment of Jessup (private communication). The present simulations are performed on coarse grids; also the crashback simulation is advanced only till approximately 35 revolutions; the results are therefore considered preliminary. Fine grid simulations for a longer period will be performed in the future.

ACKNOWLEDGEMENTS

This work was supported by the United States Office of Naval Research under ONR Grant N00014-02-1-0978 with Dr. Ki-Han Kim as technical monitor. Computing resources were provided by the National Center for Supercomputing Applications, the San Diego Supercomputing Center and the Minnesota Supercomputing Institute. We are grateful to Dr. Stuart Jessup for providing us with experimental data, and for useful discussions.

REFERENCES

[1] C.-W. Jiang, R. R. Dong, H.-L. Liu, M.-S. Chang: 24-inch water tunnel flow field measurements during propeller crashback. 21st Symposium on Naval Hydrodynamics, 1997.

[2] S. Jessup, C. Chesnakas, D. Fry, M. Donnelly, S. Black, J. Park: Propeller performance at extreme off design conditions. 25th Symposium on Naval Hydrodynamics, St. Johns, Newfoundland and Labrador, 2004.

[3] B. Chen, F. Stern: Computational fluid dynamics of four-quadrant marine-propulsor flow. Journal

of Ship Research 43 (4), 1999, 218–228.

[4] F. Davoudzadeh et al.: Coupled Navier-Stokes and equations of motion simulation of submarine maneuvers, including crashback. ASME Fluids Engineering Division Summer Meeting, Vancouver, British Columbia, Canada, 1997.

[5] H. McDonald, D. Whitfield: Self-propelled maneuvering underwater vehicles. 21st Symposium on Naval Hydrodynamics, Trondheim, Norway, 1996, 478–489.

[6] S. Jessup: An experimental investigation of viscous aspects of propeller blade flow. PhD Thesis, The Catholic University of America, Washington, D.C., 1989.

[7] C.-W. Jiang, T. T. Huang, R. Ng, Y. S. Shin: Propeller hydrodynamic loads and blade stresses and deflections during backing and crashback operations. SNAME Propellers/Shafting '91, Virginia Beach, 1991.

[8] M. Beddhu, L. K. Taylor, D. L. Whitfield: Strong conservative form of the incompressible Navier-Stokes equations in a rotating frame with a solution procedure. J. of Computational Physics 128, 1996, 427–437.

[9] K. S. Majety: Solutions to the Navier-Stokes equations in a non-inertial reference frame. MS Thesis, Mississippi State University, 2003.

[10] M. Germano, U. Piomelli, P. Moin, W. H. Cabot: A dynamic subgrid-scale eddy viscosity model. Phys. Fluids A 3 (7), 1991, 1760–1765.

[11] D. K. Lilly: A proposed modification of the Germano subgrid-scale closure method, Phys. Fluids A 4 (3), 1992, 633–635.

[12 K. Mahesh, G. Constantinescu, P. Moin: A numerical method for large-eddy simulation in complex geometries. J. Comput. Phys. 197, 2004, 215–240.

[13] R. Hecker, K. Remmers: Four quadrant open-water performance of propellers 3710, 4024, 4086, 4381, 4382, 4383, 4384 and 4426. NSRADC 417-H01, 1971.

[14] F. Di Felice, G. Romano, M. Elefante: Propeller wake analysis by means of PIV. 23rd Symposium on Naval Hydrodynamics, 2001.